

Determination of g -factor in InAs two-dimensional electron system by capacitance spectroscopy*

Hiroshi Irie, Takafumi Akiho, and Koji Muraki

NTT Basic Research Laboratories, NTT Corporation, 3-1 Morinosato-Wakamiya, Atsugi 243-0198, Japan

(Dated: March 18, 2022)

We determine the effective g -factor ($|g^*|$) of a two-dimensional electron gas (2DEG) using a new method based on capacitance spectroscopy. The capacitance-voltage profile of a 2DEG in an InAs/AlGaSb quantum well measured in an in-plane magnetic field shows a double-step feature that indicates the Zeeman splitting of the subband edge. The method allows for simultaneous and independent determination of $|g^*|$ and effective mass m^* . Data suggest that the biaxial tensile strain in the InAs layer has considerable impacts on both m^* and g^* . Our method provides a means to determine $|g^*|$ that is complementary to the commonly used coincidence technique.

The electron g -factor is a fundamental quantity that governs the coupling between the spin degree of freedom and external magnetic fields. In the solid state, the g -factor is altered from its value in vacuum ($g_e \approx 2$) by spin-orbit coupling and can even change sign, thus becoming a material-dependent parameter referred to as the effective g -factor, denoted as g^* . This coupling, making g^* dependent on various parameters such as electric field and quantum confinement, allows for controlling the spin degree of freedom by electrical means, which forms the basis for spintronics and quantum information processing.¹ Recently, the combination of the strong spin-orbit interaction inherent in narrow-gap semiconductors and external magnetic fields has proven to provide routes to the emergent quantum phase,^{2,3} where g^* plays an important role. In a two-dimensional electron gas (2DEG), a common platform for various nanostructures and hybrid devices, g^* is determined by a method known as the coincidence technique.⁴⁻⁷ The method uses magnetic field B , with the angle θ from the sample normal varied to tune the ratio r ($= |g^*| m^* / \hbar e \cos \theta$) between the Zeeman splitting $E_Z = |g^*| \mu_B B$ and cyclotron energy $\hbar e B_\perp / m^*$, where μ_B is the Bohr magneton, \hbar is Planck's constant divided by 2π , e is the elementary charge, $B_\perp = B \cos \theta$ is the perpendicular component of B , and m^* is the effective mass. Then $|g^*|$ is known from θ at which particular resistance minima disappear due to level coincidence. However, in the presence of B_\perp , electron-electron interaction can affect g^* in a manner dependent on the Landau-level filling factor.^{6,8} Therefore, alternative means to determine $|g^*|$ without B_\perp , which can provide complementary information, will be helpful. In this study, we present a new method based on capacitance spectroscopy that does not require B_\perp and determine $|g^*|$ of a 2DEG in a quantum well (QW) of InAs, a narrow-gap semiconductor with strong spin-orbit interaction and large $|g^*|$.

Our method is based on the measurement of quantum capacitance $c_Q = e^2 (dn_s / d\mu)$, which is proportional to the thermodynamic density of states (DOS) $\mathcal{D} = dn_s / d\mu$ of the 2DEG^{9,10} [Fig. 1(a)]. Here, μ is the chemical potential, and n_s is the electron density. We apply a strong in-plane magnetic field B_\parallel and measure the Zeeman splitting of the subband edge [Fig. 1(b)] that appears as a double step in the capacitance-voltage profile. Figure 2(a) shows the equivalent-circuit representation of the system. The differential capacitance c_{FG} (per unit area) between the 2DEG and the front gate, separated by an insulator with dielectric constant ϵ_b and thickness

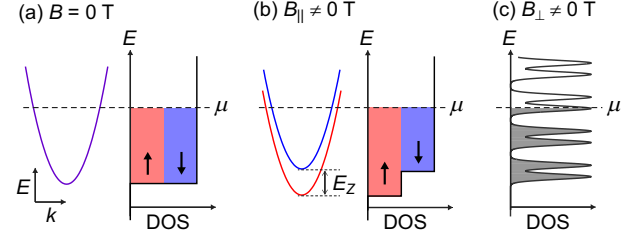


FIG. 1. Schematic illustrations of band dispersion and density of states of a two-dimensional electron gas subjected to (a) zero, (b) in-plane, and (c) perpendicular magnetic fields.

d_b , can be described by a series sum of c_Q and geometrical capacitance $c_G = \epsilon_b / d_b$ as

$$c_{FG}^{-1} = c_G^{-1} + c_Q^{-1}. \quad (1)$$

Using this equation along with $e(dn_s / dV_{FG}) = c_{FG}$, where V_{FG} is the front-gate voltage, one can show that the relation

$$\mu = e \int_{V_{th}}^{V_{FG}} \left[1 - \frac{c_{FG}(V'_{FG})}{c_G} \right] dV'_{FG} \quad (2)$$

holds between μ and V_{FG} ,¹¹ where V_{th} is the threshold voltage at which the 2DEG starts to accumulate. This relation can be used to translate voltage into energy from the measured c_{FG} vs V_{FG} . This allows us to obtain E_Z (and hence $|g^*|$) from the double-step feature in the capacitance-voltage profile.

Measurements were conducted at 1.8 K on a square ($600 \mu\text{m} \times 590 \mu\text{m}$) device fabricated from a heterostructure grown by molecular beam epitaxy on an n -type GaSb (001) substrate. Figure 2(c) depicts the layer structure of the device. The 2DEG is hosted in a 20-nm-wide InAs QW sandwiched by 10-nm-thick $\text{Al}_{0.7}\text{Ga}_{0.3}\text{Sb}$ barriers. The QW structure is flanked on both sides by outer $\text{AlAs}_{0.08}\text{Sb}_{0.92}$ barrier layers and capped with 5-nm GaSb. The $\text{AlAs}_{0.08}\text{Sb}_{0.92}$ layers were designed to lattice-match the GaSb substrate and thereby eliminate dislocation formation. Note that the lattice constant of InAs ($\text{Al}_{0.7}\text{Ga}_{0.3}\text{Sb}$), 6.0501 (6.1139) Å, is 0.52% smaller (0.53% larger) than that of GaSb (6.0817 Å). This induces a biaxial 0.52% tensile (0.53% compressive) strain in the InAs ($\text{Al}_{0.7}\text{Ga}_{0.3}\text{Sb}$) layer(s). The device has two Ohmic contacts and a front gate with a 40-nm-thick Al_2O_3 insulator atomic-layer deposited on the heterostructure. We measured the capacitance C_{exp} between the front gate and the 2DEG¹² using a

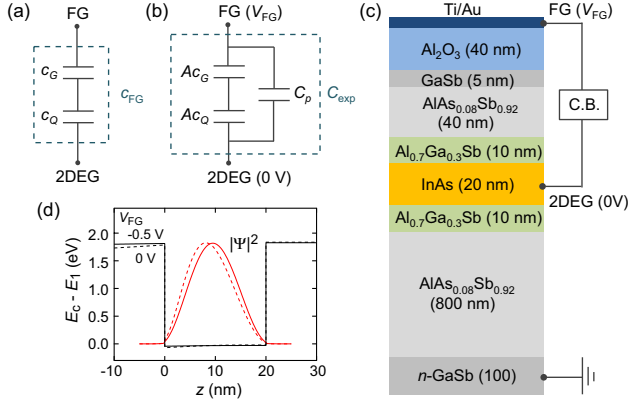


FIG. 2. (a) Equivalent-circuit representation of the differential capacitance c_{FG} (per unit area) between the front gate and 2DEG. (b) Equivalent circuit for differential capacitance C_{exp} measured in the experiment. (c) Layer structure of the device with a connection diagram for the capacitance-bridge (C.B.) measurement. (d) Profiles of the conduction-band edge $E_c(z)$ measured from the lowest sub-band energy E_1 and squared envelope function $|\Psi(z)|^2$ calculated for $V_{FG} = -0.5$ (solid lines) and 0 V (dashed lines).

capacitance bridge (Andeen-Hagerling 2700A) as a function of V_{FG} [Fig. 2(c)], at a frequency of 320 Hz and an excitation voltage of 3 mVrms. The dissipation factor measured simultaneously with C_{exp} was negligibly small for the V_{FG} range studied, which confirms the irrelevance of charge trapping in the barrier layers. The underlying n -GaSb (buffer layer and substrate) was electrically isolated from the 2DEG by the thick $AlAs_{0.08}Sb_{0.92}$ layer, and therefore did not contribute to C_{exp} . Separate transport measurements on a Hall-bar device fabricated from the same wafer showed that the 2DEG had sheet density of $n_s = 3.65 \times 10^{15} \text{ m}^{-2}$ and low-temperature mobility of $50 \text{ m}^2/\text{Vs}$ at $V_{FG} = 0 \text{ V}$. Self-consistent envelope-function calculations reveal a slightly asymmetric charge distribution within the QW with negligible penetration into the $AlGaSb$ barriers for the V_{FG} range relevant to the $|g^*|$ determination [Fig. 2(d)]. A magnetic field of up to 14 T was applied either parallel or perpendicular to the 2DEG.

In actual experiments, parasitic capacitance C_p exists, which enters in parallel [Fig. 2(b)]. In addition, c_G is not perfectly constant and varies with V_{FG} as shown below. Therefore, we first show how we determined C_p and c_G by presenting the data obtained at zero magnetic field ($B = 0 \text{ T}$) and in a perpendicular field B_{\perp} . Figure 3(a) shows the measured C_{exp} as a function of V_{FG} . At $B = 0 \text{ T}$, C_{exp} is nearly constant at $V_{FG} > -0.8 \text{ V}$, and decreases sharply when the 2DEG is depleted at $V_{FG} \leq -0.8 \text{ V}$. As eq. (1) shows, this sharp decrease represents the contribution of c_Q to c_{FG} . In the depletion region ($V_{FG} \leq -0.8 \text{ V}$), C_{exp} takes a finite value, corresponding to the parasitic capacitance, which mainly stems from the overlap between the front gate and Ohmic electrodes.

When a perpendicular field is applied, the DOS of the 2DEG splits into a series of peaks due to Landau quantization [Fig. 1(c)]. Accordingly, C_{exp} oscillates as a function of V_{FG} , where the high (low) C_{exp} indicates that the Fermi level lies within a Landau level (between Landau levels).¹⁴ Notably,

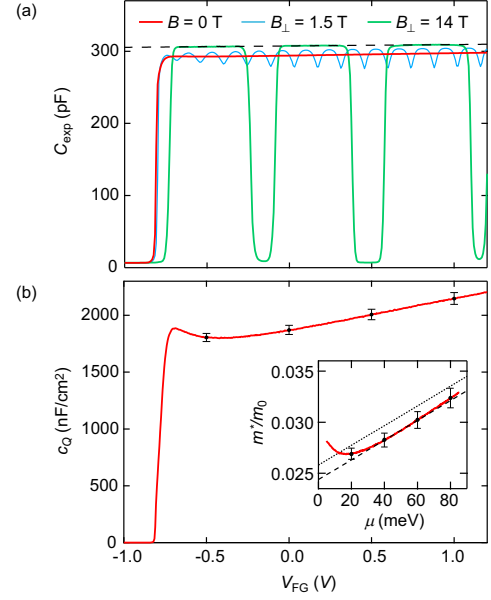


FIG. 3. (a) Capacitance-voltage profile measured at $B_{\perp} = 0, 1.5$, and 14 T. The dashed line is a linear fit to the flattened top parts of the $B_{\perp} = 14 \text{ T}$ data, representing the geometrical capacitance Ac_G . (b) c_Q obtained from C_{exp} at $B = 0 \text{ T}$. Inset shows the effective mass calculated from c_Q (solid line). The error bars represent the maximum error caused by the linear approximation of c_G vs V_{FG} . The dashed and dotted lines are theoretical values for a 20-nm-wide InAs QW with and without strain effects taken into account, respectively, taken from Ref. 13.

maxima of C_{exp} flatten out at a very high field ($B_{\perp} = 14 \text{ T}$). This happens because, at high fields, the large DOS of Landau levels makes c_Q much greater than c_G ; consequently, the second term in eq. (1) becomes negligible.¹⁵ Hence, we have $C_{exp} \approx Ac_G + C_p$, where $A (= 0.347 \text{ mm}^2)$ is the area of the 2DEG.¹⁶ In turn, this implies that, once C_p is known, c_G can be determined experimentally by measuring C_{exp} at a sufficiently strong B_{\perp} where $c_Q \gg c_G$.¹⁷ In the following analysis, we use the value $C_p = 6.8 \text{ pF}$, which we confirmed to be constant at high B_{\perp} .¹⁸

As shown by the dashed line in Fig. 3(a), the C_{exp} values in the flat-top regions can be fitted by a single straight line. The fit line has a finite slope, which indicates that c_G slightly increases with V_{FG} . This is because the 2DEG has a finite width, and its centroid $\langle z \rangle$ within the QW varies with V_{FG} , reflecting the change in the confinement potential.^{10,19} This effect can be incorporated by representing c_G as

$$c_G^{-1} = \frac{d_b}{\epsilon_b} + \frac{\gamma \langle z \rangle}{\epsilon_s}, \quad (3)$$

where $\langle z \rangle$ is measured from the upper interface, ϵ_s is the dielectric constant of the QW, and γ is a numerical prefactor typically 0.5–0.7.¹⁹ In the following analysis, we used a linear fit function, like that in Fig. 3(a), to determine c_G as a function of V_{FG} . This allows us to extract c_Q from c_{FG} using eq. (1) without the need for knowledge of γ and $\langle z \rangle$. The linear fit agrees with C_{exp} to within 0.3 pF, with the corresponding

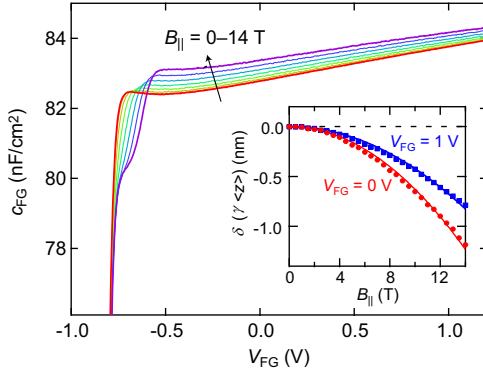


FIG. 4. c_{FG} as a function of V_{FG} measured at zero and various in-plane magnetic fields ($B_{\parallel} = 0$ –14 T with intervals of 2 T). Inset shows the shift of the wave-function centroid with B_{\parallel} estimated from the B_{\parallel} dependence of c_{FG} at $V_{FG} = 0$ and 1 V (symbols). Lines are quadratic fit.

errors in c_Q and μ estimated to be less than $\pm 3\%$.

Figure 3(b) plots c_Q obtained from the C_{exp} data at $B = 0$ T as a function of V_{FG} . The c_Q shows a sharp onset at $V_{FG} = -0.8$ V, where the 2DEG appears, and increases slowly with V_{FG} at a nearly constant slope, except in the vicinity of the onset. To check the validity of our analysis, we calculated m^* from c_Q using the relation $dn_s/d\mu = m^*/\pi\hbar^2$ and compared it with the existing theoretical models¹³ for m^* [inset of Fig. 3(b)]. The horizontal axis is the energy measured from the subband edge E_1 . The experimental data are plotted vs μ obtained using eq. (2), with $\mu = 0$ defined as the middle point of the step edge in the c_Q vs μ [see Fig. 5(a)]. The experimentally obtained m^* increases with μ , with the slope in good agreement with the model accounting for the nonparabolicity of the InAs conduction band (dotted line). The quantitative agreement with theory is significantly improved when the effects of the 0.52% in-plane tensile strain in the InAs layer are taken into account (dashed line).^{13,20} The deviation from the linear dependence near the subband edge suggests electron-electron interaction that becomes important at low densities, which will be discussed later. We emphasize, however, that the determination of $|g^*|$ using eq. (2) is not affected by the value of m^* obtained in our method, for it holds irrespective of the m^* value.

Now we present results obtained with magnetic field B_{\parallel} applied parallel to the 2DEG. Figure 4 plots c_{FG} vs V_{FG} for $B_{\parallel} = 0$ –14 T. The data reveal that at large B_{\parallel} an extra step feature develops near the onset, indicating the Zeeman splitting of the subband edge, as illustrated in Fig. 1(b). As expected, the step becomes wider as B_{\parallel} increases. It is worth noting that, aside from the double-step feature, c_{FG} is seen to vary with B_{\parallel} also in the high- V_{FG} range away from the subband edges. This behavior, not expected from a simple picture, has previously been identified and explained as due to the B_{\parallel} -induced shift of the wave-function centroid in an asymmetric confinement potential.^{19,21,22} To quantify the shift, we translated the change in c_{FG} at each V_{FG} with respect to its $B_{\parallel} = 0$ value into $\gamma\langle z \rangle$, which we plot in the inset as a function of B_{\parallel} for $V_{FG} = 0$ and

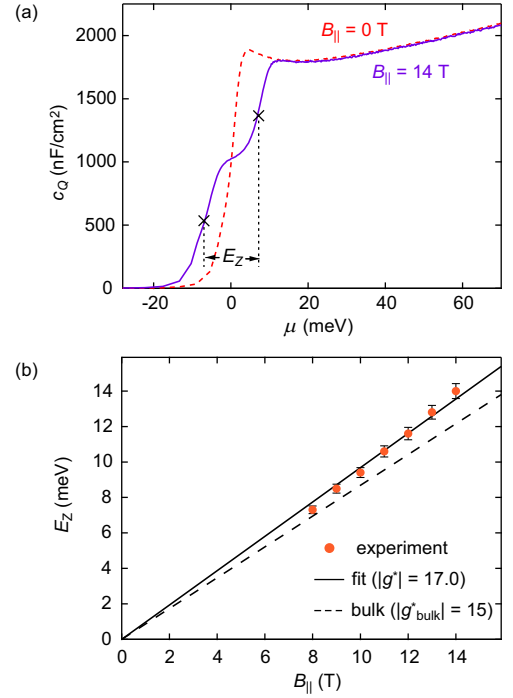


FIG. 5. (a) c_Q at $B_{\parallel} = 0$ and 14 T as a function of μ . Crosses indicate the middle of the step edges where the Fermi level is aligned to the subband edge. E_Z is deduced from the difference in μ 's at these two points. $\mu = 0$ for the $B_{\parallel} = 14$ T data is set at the midpoint of these two points. (b) E_Z determined for various in-plane fields, plotted vs B_{\parallel} . Open circles show experimental data. The error bars indicate the error associated with the uncertainty ($\pm 3\%$) in μ . The solid line is a linear fit to the experimental data. For comparison, E_Z calculated using the g -factor of bulk InAs is shown by dashed line.

1 V. The shift can be fitted well with a quadratic function as $\delta\langle\gamma\langle z \rangle\rangle = \alpha B_{\parallel}^2$. The prefactor α is found to be V_{FG} dependent, and can be expressed as $\alpha = (6.20 - 2.05V_{FG}) \times 10^{-3}$ nm/T². Once the centroid shift is absorbed in the B_{\parallel} dependence of c_G , c_Q in the high- μ region is no longer B_{\parallel} dependent, as shown in Fig. 5(a), where we plot c_Q at $B_{\parallel} = 0$ and 14 T as a function of μ .²³ The double steps of c_Q at $B_{\parallel} = 14$ T are nearly equal in height, consistent with the equal DOS for the up and down spin states. If we assume that the Fermi level aligns with the subband bottom at the middle of the step edges [crosses in Fig. 5(a)], we can deduce the energy difference E_Z from their separation. Note that the step edges are broadened by disorder, most likely due to background charged impurities, which limits the minimum resolvable E_Z to ~ 7 meV in the present experiment.

Figure 5(b) plots E_Z determined for each B_{\parallel} . Linear fitting of E_Z vs B_{\parallel} yields $|g^*| = 17.0 \pm 0.5$. Notably, this $|g^*|$ value is larger than that of bulk InAs ($g_{bulk}^* = -15$).^{24,25} In QWs, g^* depends on the well width, reflecting the quantum confinement, which can be understood in terms of the energy dependence of g^* . With the Kane model,²⁶

$$g^*(E) = g_e - \frac{2E_P}{3} \frac{\Delta}{(E_g + E)(E_g + E + \Delta)}, \quad (4)$$

where E is the energy measured from the bottom of the bulk conduction band E_c , E_g is the band gap, Δ is the spin-orbit splitting of the valence band, and $E_P = 2m_0P^2/\hbar^2$ with m_0 the electron mass in vacuum and P the Kane momentum-matrix element. With the parameters for InAs ($E_g = 0.417$ eV, $\Delta = 0.39$ eV, and $E_P = 21.5$ eV),²⁷ eq. (4) predicts that g^* varies from -14.6 at the conduction-band bottom ($E = 0$) to, e.g., $g^* = -12.9$ at $E = 0.03$ eV. The reported value $|g^*| \approx 13$ for a 15-nm-wide InAs/AlSb QW, obtained using the coincidence technique,⁷ can therefore be explained by eq. (4) if the Fermi level lies ~ 0.03 eV above the conduction-band bottom of bulk InAs. However, quantum confinement cannot account for $|g^*|$ greater than the bulk value we observed. We estimate $E \sim 0.03$ eV in our 20-nm-wide QW due to quantum confinement ($\langle E_1 - E_c(z) \rangle \sim 0.03$ eV), which would yield $g^* = -12.9$. As we argue below, the reduction of E_g due to biaxial tensile strain can override the effects of E on g^* . If we take the energy of the light-hole band, which is at the top of the valence band for biaxial tension,¹³ we find that the 0.52% strain decreases E_g of InAs by 0.068 eV (parameters are from Ref. 27). Applying this value to eq. (4) together with $E \sim 0.03$ eV, we have $g^* = -17.2$. Although a more elaborate theory, as that for m^* in Ref. 13, is required for a rigorous discussion, our result suggests that the strain effect on g^* is important in heterostructures as well as in nanowires and quantum dots; it can be comparable to or even override the effects of quantum confinement for the case of tensile strain and therefore must be taken into account to discuss subtle effects,

such as electron-electron interaction that becomes important at low density.²⁸

We point out several differences between our method and the coincidence technique. Firstly, the latter provides only the product $|g^*|m^*$; hence, an accurate determination of $|g^*|$ requires precise knowledge of m^* . This is not the case for our method; as we demonstrated in this study, it allows for simultaneous and independent determination of m^* and $|g^*|$. Yet, our method requires large $|g^*|$ for the double-step feature to be resolved in the capacitance-voltage profile. Secondly, in our method, $|g^*|$ is determined at a rather low electron density at which the upper-spin subband is depopulated and the system becomes fully spin polarized. The corresponding n_s depends on $|g^*|m^*$ and B_{\parallel} . In the present case of InAs, where $|g^*|m^*/m_0 \sim 0.46$ leads to a rather large n_s of $\sim 1 \times 10^{15} \text{ m}^{-2}$ at $B_{\parallel} = 14$ T, this value is still much smaller than the typical densities in coincidence experiments. Thirdly, while the coincidence technique assumes g^* to be isotropic, our method selectively measures the in-plane g -factor. These differences will allow our method to provide information complementary to coincidence experiments and make it useful in some situations, such as for investigating the effects of electron-electron interaction on m^* and $|g^*|$ in the absence of perpendicular magnetic fields.

Acknowledgements The authors thank Hiroaki Murofushi for processing the device. This work was supported by JSPS KAKENHI Grant No. JP15H05854.

-
- * Published in Applied Physics Express on May 20, 2019. H. Irie, T. Akiho, and K. Muraki, *Appl. Phys. Express* **12** 063004 (2019). This Accepted Manuscript is available for reuse under a CC BY-NC-ND 3.0 licence after the 12 month embargo period provided that all the terms and conditions of the licence are adhered to.
- ¹ M. W. Wu, J. H. Jiang, and M. Q. Weng, *Phys. Rep.* **493**, 61 (2010).
 - ² J. Alicea, *Reports Prog. Phys.* **75**, 076501 (2012).
 - ³ H. J. Suominen, M. Kjaergaard, A. R. Hamilton, J. Shabani, C. J. Palmström, C. M. Marcus, and F. Nichele, *Phys. Rev. Lett.* **119**, 176805 (2017).
 - ⁴ F. F. Fang and P. J. Stiles, *Phys. Rev.* **174**, 823 (1968).
 - ⁵ T. P. Smith III and F. F. Fang, *Phys. Rev. B* **35**, 7729 (1987).
 - ⁶ R. J. Nicholas, R. J. Haug, K. v. Klitzing, and G. Weimann, *Phys. Rev. B* **37**, 1294 (1988).
 - ⁷ S. Brosig, K. Ensslin, A. G. Jansen, C. Nguyen, B. Brar, M. Thomas, and H. Kroemer, *Phys. Rev. B* **61**, 13045 (2000).
 - ⁸ T. Ando and Y. Uemura, *J. Phys. Soc. Japan* **37**, 1044 (1974).
 - ⁹ S. Luryi, *Appl. Phys. Lett.* **52**, 501 (1988).
 - ¹⁰ A. Ali, H. Madan, R. Misra, A. Agrawal, P. Schiffer, J. B. Boos, B. R. Bennett, and S. Datta, *IEEE Trans. Electron Devices* **58**, 1397 (2011).
 - ¹¹ V. S. Khrapai, A. A. Shashkin, M. G. Trokina, V. T. Dolgoplov, V. Pellegrini, F. Beltram, G. Biasiol, and L. Sorba, *Phys. Rev. Lett.* **99**, 086802 (2007).
 - ¹² Throughout this paper, we use the upper case C to denote capacitance to distinguish it from capacitance per area c denoted in the lower case.
 - ¹³ P. J. Lin-Chung and M. J. Yang, *Phys. Rev. B* **48**, 5338 (1993).
 - ¹⁴ T. P. Smith, B. B. Goldberg, P. J. Stiles, and M. Heiblum, *Phys. Rev. B* **32**, 2696 (1985).
 - ¹⁵ G. L. Yu, R. Jalil, B. Belle, A. S. Mayorov, P. Blake, F. Schedin, S. V. Morozov, L. A. Ponomarenko, F. Chiappini, S. Wiedmann, U. Zeitler, M. I. Katsnelson, A. K. Geim, K. S. Novoselov, and D. C. Elias, *Proc. Natl. Acad. Sci. U. S. A.* **110**, 3282 (2013).
 - ¹⁶ We estimated A by comparing the density obtained by numerically integrating the measured capacitance and that determined from the magneto-capacitance oscillations for $B_{\perp} = 1\text{--}2$ T at various V_{FG} . The 2% reduction from the lithographic size is likely due to overetching of the mesa side walls.
 - ¹⁷ A simple calculation shows that $c_Q/c_G \geq 100$ is satisfied for Gaussian Landau-level broadening of $\sigma \leq 2.4$ meV at $B_{\perp} = 14$ T for our sample geometry.
 - ¹⁸ This value agrees well with the minimum of C_{exp} at $V_{\text{FG}} = 0.5$ V, which corresponds to the integer quantum Hall effect at Landau-level filling factor 2, where the DOS at the Fermi level is expected to become minimum.
 - ¹⁹ J. Hampton, J. Eisenstein, L. Pfeiffer, and K. West, *Solid State Commun.* **94**, 559 (1995).
 - ²⁰ M. J. Yang, P. J. Lin-Chung, B. V. Shanabrook, J. R. Waterman, R. J. Wagner, and W. J. Moore, *Phys. Rev. B* **47**, 1691 (1993).
 - ²¹ F. Stern, *Phys. Rev. Lett.* **21**, 1687 (1968).
 - ²² T. Jungwirth and L. Smrčka, *Phys. Rev. B* **51**, 10181 (1995).
 - ²³ The error in μ associated with the parabolic approximation of c_{FG} vs B_{\parallel} (Fig. 4 inset) is negligible compared to that associated with the linear approximation of c_G vs V_{FG} [Fig. 3(a)].

- ²⁴ C. R. Pidgeon, D. L. Mitchell, and R. N. Brown, [Phys. Rev. **154**, 737 \(1967\)](#).
- ²⁵ J. Konopka, Phys. Lett. A **26**, 29 (1967).
- ²⁶ A. A. Kiselev, E. L. Ivchenko, and U. Rössler, [Phys. Rev. B **58**, 16353 \(1998\)](#).
- ²⁷ I. Vurgaftman, J. R. Meyer, and L. R. Ram-Mohan, [J. Appl. Phys. **89**, 5815 \(2001\)](#).
- ²⁸ A. Tsukazaki, A. Ohtomo, M. Kawasaki, S. Akasaka, H. Yuji, K. Tamura, K. Nakahara, T. Tanabe, A. Kamisawa, T. Gokmen, J. Shabani, and M. Shayegan, [Phys. Rev. B **78**, 233308 \(2008\)](#).